arXiv:hep-ex/0306046v1 22 Jun 2003

THE CDF EXPERIMENT AT THE TEVATRON —
THE FIRST TWO YEARS OF RUN II*

ARND MEYER

III. Physikalisches Institut A, RWTH Aachen, Physikzentrum
52056 Aachen, Germany
meyera@fnal.gov

For the CDF Collaboration

The 1992-1995 running of the Fermilab Tevatron (the so-called Run I) ended with many important physics goals accomplished, including the discovery of the top quark, and the anticipation of many further questions to be answered in the future. After many upgrades to the detector and to the accelerator complex, Run II began in April 2001. First results obtained by the Collider Detector at Fermilab (CDF) collaboration from the analysis of early Tevatron Run II data are reported here. They fall in two categories: a number of measurements have been performed with the primary goal of establishing detector performance and physics potential. Another set of measurements make use of completely new capabilities of the upgraded detector, thus allowing for competitive results with a modest amount of integrated luminosity.

1. Introduction

There have been numerous tantalizing suggestions, both experimental and theoretical, that physics beyond the Standard Model might be within our reach. After the very successful Tevatron Run I (1992-1995), colliding protons and antiprotons with a center of mass energy of $\sqrt{s} = 1.8$ TeV, the accelerator and the colliding beam experiments CDF and DØ were upgraded for Run II, in order to expand the reach toward whatever new physics might exist.

On the accelerator side, the beam energy has been increased from 900 GeV to 980 GeV. For some rare processes like $t\bar{t}$ production this modest increase translates into a cross section higher by 30% or more. In Run I the luminosity reached $1.5 \cdot 10^{31} \mathrm{cm}^{-2}\mathrm{s}^{-1}$, while the ultimate goal for Run II is $2-4\cdot10^{32}\mathrm{cm}^{-2}\mathrm{s}^{-1}$. A new proton storage ring, the "Main Injector", has been built, and the same tunnel houses the "Recycler" storage ring, which will improve the rate at which antiprotons can be

---

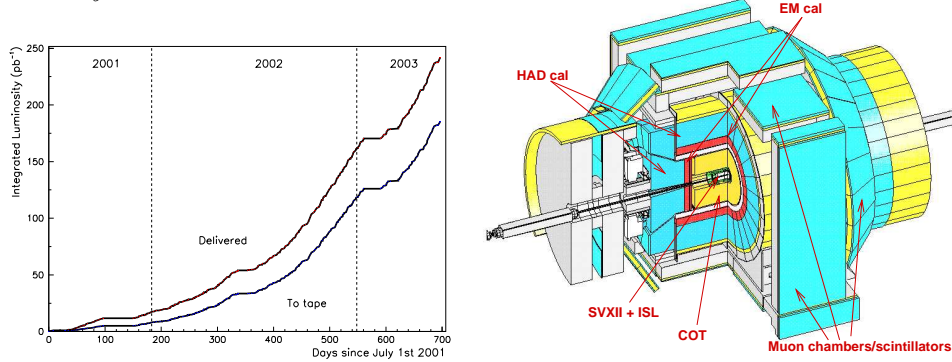*Talk given at the DESY "Tuesday seminar" in November 2002

Fig. 1.   *Left:* Delivered and recorded luminosity for CDF during early Run II. *Right:* Schematic of the CDF Run II detector.

accumulated, and may also be utilized to reuse antiprotons after recovering them from the Tevatron. The bunch spacing in the Tevatron has been reduced from $3.5\,\mu$s to 396 ns, corresponding to 36 colliding proton and antiproton bunches, mostly to keep the number of overlapping events in the experiments small.

By June 2003, the Tevatron routinely achieved peak luminosities of $4 - 5 \cdot 10^{31}$ cm^{-2}s^{-1}. The integrated luminosity delivered to CDF between July 2001 and June 2003 amounts to $240\,$pb^{-1}, and CDF recorded about $185\,$pb^{-1} (Fig. 1). The detector has been fully functional since early 2002, and the results shown below are based on up to $85\,$pb^{-1} collected mostly in 2002, a data sample comparable to the Run I data set ($\int \mathcal{L}\, dt \simeq 110\,$pb^{-1}).

Run II will be split into two major periods of data taking: Run IIa, which is scheduled to last until the end of 2005, should provide at least $2\,$fb^{-1} of integrated luminosity. Run IIb will last until the beginning of the LHC physics program, bringing the total data sample to about $10\,$fb^{-1}.

2. Detector and Trigger

The CDF detector (Fig. 1) is designed for general purpose use, with a large tracking system inside a uniform $1.4\,$T solenoidal magnetic field, 4π calorimetry, and a muon detection system. A detailed description of the CDF upgrade project for Run II can be found in Ref. 1. The entire tracking system (Fig. 2) has been replaced for Run II. The Silicon tracking system consists of three main components, such that a typical particle traverses seven layers of Silicon at radii of 1.5 cm to 28 cm. Its main purpose is the precise measurement of secondary vertices from b decays. Next, the Central Outer Tracker (COT) is an open cell drift chamber for the precise momentum measurement of charged tracks, using up to 96 space points, and with an efficiency of close to 100% for high p_T isolated tracks. Between the COT and the solenoid is the new Time-of-Flight detector (TOF), with a time resolution of 100 ps and consisting of 216 about 3m long scintillator bars, which together with the momentum measurement provides particle identification by determining a particle's
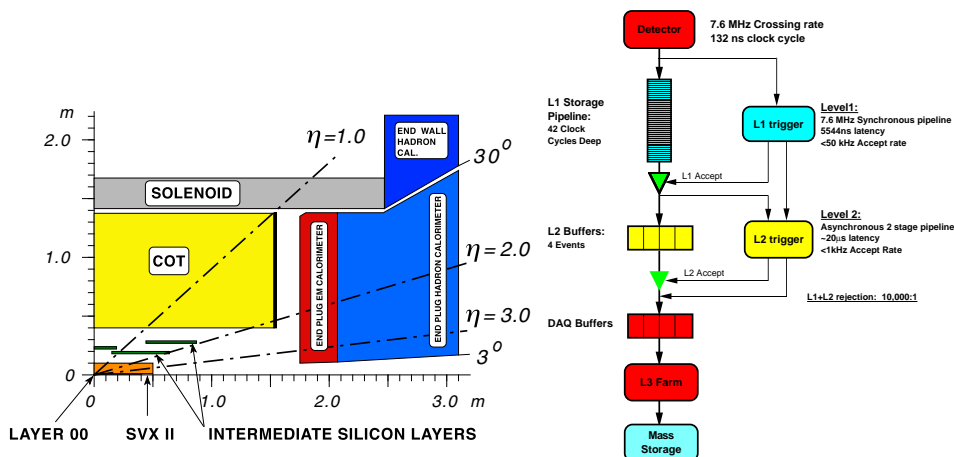
Fig. 2. *Left:* Side view of the tracking system. *Right:* The CDF trigger system for Run II.

mass. Electromagnetic and hadronic calorimeters are situated outside the solenoid. Electrons, photons, and jets deposit almost all their energy in the calorimeters. Muons travel through the calorimeters depositing only a small fraction of their energy, and are detected by the muon chambers which surround the calorimeters and steel absorbers. The luminosity is measured with two modules of 48 low-mass Cherenkov counters, covering the rapidity region from 3.75 to 4.75, by counting the rate of inelastic $p\bar{p}$ interactions, and verified with measurements of well known physics processes like W production.

The three-level trigger system and the data acquisition system[2] have been significantly enhanced for Run II (Fig. 2). The Level 1 trigger is fully pipelined with a depth of 42×132 ns, mostly based on custom-built hardware, and delivers a decision every 132 ns. The following trigger levels are highly buffered, and the event digitization and readout does not interrupt triggering, so that the entire system is to first order deadtime-free. The first trigger level provides fast drift chamber tracks with high precision and efficiency, muon and electron triggers based on signatures in the muon chambers and calorimeter in combination with drift chamber tracks, and calorimeter based triggers looking for missing transverse energy, photons, and jets. The Level 1 accept rate achieved to date is about 20 kHz. At the second trigger level the rate is reduced with the help of refined information from all detector components. The major part of the rate reduction at Level 2 to about 300 Hz is provided by the secondary vertex trigger, using information from the Silicon system. The third trigger level consists of a conventional farm of Linux PC's. A filter program based on an optimized version of the regular reconstruction program reduces the rate to typically 50 Hz which are written to permanent storage (disk and tape).

3. Charm and Beauty

Traditionally heavy flavor physics at hadron colliders relies on a lepton signature; examples are the decay of the J/ψ into $\mu^+\mu^-$ or semileptonic b decays. With the Silicon Vertex Tracker (SVT)[3] CDF has introduced a novel method to obtain heavy flavor decays. The SVT uses COT tracks as seeds to a parallelized pattern recognition in the Silicon vertex detector. The following linearized track fit returns track parameters with nearly offline resolution on a time scale of $15\,\mu$s. The precise measurement of the track impact parameter ($\simeq 50\,\mu$m including a $\simeq 35\,\mu$m contribution from the transverse size of the beams) makes it possible to trigger on displaced tracks from long-lived hadrons containing heavy flavor. Originally designed to select hadronic B decays the SVT also collects a large sample of charm hadrons.

3.1. *Charm*

All of the charm measurements shown here, with the exception of the J/ψ cross section, are based on data samples collected with the SVT.

3.1.1. *Prompt D Meson Cross Sections*

There is no published measurement of the charm cross section from the Tevatron. With the advent of the SVT this measurement is possible in Run II, and it is of theoretical interest due to the larger than expected beauty cross sections compared to next-to-leading order QCD calculations. The measurement shown here, based on the analysis of $5.8\,\mathrm{pb}^{-1}$ of data, makes use of four fully reconstructed decay modes: $D^0 \to K^-\pi^+$, $D^{*+} \to D^0\pi^+$ with $D^0 \to K^-\pi^+$, $D^+ \to K^-\pi^+\pi^+$, and $D_s^+ \to \phi\pi^+$ with $\phi \to K^+K^-$. The mass spectra are shown in Fig. 3.

The contributions from prompt and secondary charm are separated by utilizing the impact parameter distribution of the reconstructed D meson samples. Mesons originating from B decays exhibit a large impact parameter. A fit to the impact parameter distribution yields prompt production fractions of $88.6 \pm 0.4(\mathrm{stat}) \pm 3.5(\mathrm{sys})\%$, $88.1 \pm 1.1 \pm 3.9\%$, $89.1 \pm 0.4 \pm 2.8\%$, and $77.3 \pm 3.8 \pm 2.1\%$ for D^0, D^+, D^+, and D_s^+, respectively, averaged over the full analyzed p_T range.

The measured prompt differential cross sections are shown in Fig. 4. They are compared to a next-to-leading order QCD calculation[4], and a fixed order next-to-leading log calculation[5]. The calculations are lower than, but compatible with the data. The total cross sections are found to be: $\sigma(D^0, p_T > 5.5\,\mathrm{GeV}) = 13.3 \pm 0.2 \pm 1.5\,\mu$b, $\sigma(D^{*+}, p_T > 6.0\,\mathrm{GeV}) = 5.4 \pm 0.1 \pm 0.8\,\mu$b, $\sigma(D^+, p_T > 6.0\,\mathrm{GeV}) = 4.3 \pm 0.1 \pm 0.7\,\mu$b, and $\sigma(D_s^+, p_T > 8.0\,\mathrm{GeV}) = 0.75 \pm 0.05 \pm 0.22\,\mu$b, where the first error is statistical, and the second covers systematic uncertainties.

3.1.2. $m_{D_s^+} - m_{D^+}$ *Mass Difference*

The measurement of the $m_{D_s^+} - m_{D^+}$ mass difference provides a test for the Heavy Quark Effective Theory and lattice QCD. While many precision measurements of
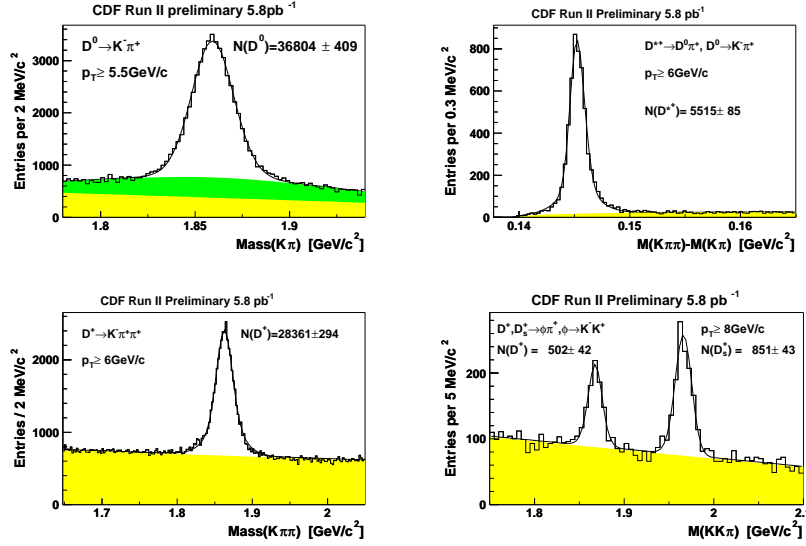
Fig. 3. Reconstructed mass spectra for the four reconstructed D meson decays. The shaded area indicates the fitted combinatorial background. For the D^0 the second shaded area shows the autoreflection contribution (exchange of K and π). The signals are parameterized by single (D^0, D_s^+, $D^+ \to K^-\pi^+\pi^+$) or double (D^{*+}, $D^+ \to \phi\pi^+$) Gaussians, respectively.
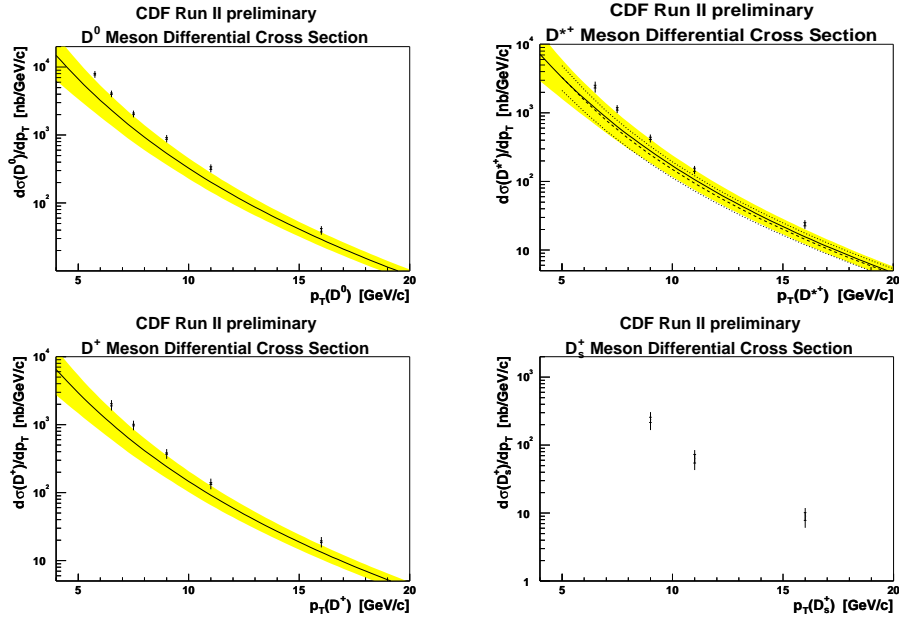

Fig. 4. Differential cross section for the four reconstructed D mesons. Theoretical predictions from Kniehl *et al.* (dashed line with dotted line indicating uncertainty) and Cacciari *et al.* (full line with shaded band as uncertainty) are compared to the data. The theoretical uncertainties are based on varying the renormalization and factorization scales independently by factors of 0.5 to 2.
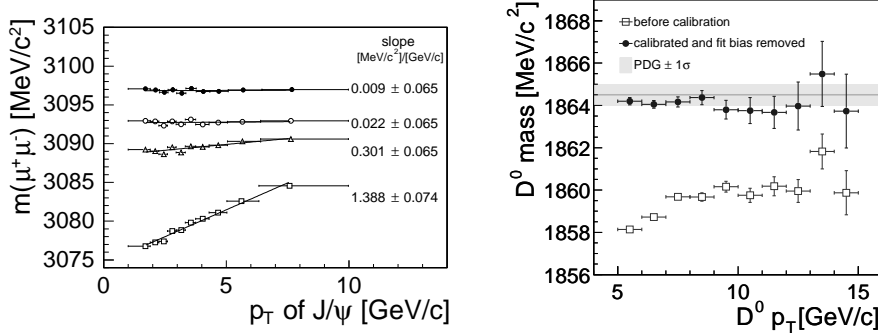
Fig. 5.   Momentum scale calibration. *Left:* Illustration of the procedure using the momentum dependence of the reconstructed J/ψ mass. The four sets of measurements are, from bottom to top: raw track reconstruction, inclusion of material effects, fine tuning of material, fine tuning of the magnetic field. *Right:* Validation with $D^0 \to K\pi$ decays.

meson masses can be expected from Run II, the analysis shown here could already be carried out with a modest amount of luminosity.

For all mass measurements a calibrated momentum scale is a key issue. A large sample of J/ψ dimuon decays was used to calibrate energy loss and magnetic field (Fig. 5). Slopes in the transverse momentum dependence of the J/ψ mass are attributed to uncorrected energy loss. The corrections are adjusted to account for material missing in the description of the detector. The overall mass shift with respect to the well measured world average J/ψ mass is used to fine tune the magnetic field. The procedure was validated using different final states (e.g. $D^0 \to K\pi$ decays shown in Fig. 5).

The mass difference measurement relies on D_s^+ and D^+ decays into $\phi\pi^+$ with $\phi \to K^+K^-$, as shown in Fig. 6. Using the same decay mode has the advantage of cancelling systematic uncertainties. The unbinned likelihood fit of the mass spectrum results in $m_{D_s^+} - m_{D^+} = 99.41 \pm 0.38(\text{stat}) \pm 0.21(\text{sys})\,\text{MeV}$, with uncertainties comparable to the world average[6]. This measurement constitutes the first published Run II result from CDF[7].

3.1.3. *Cabibbo Suppressed Decays and CP Violation*

Utilizing the huge sample of D^0 mesons in 65 pb^{-1} integrated luminosity collected with the secondary vertex trigger, relative branching fractions are measured, $\frac{\Gamma(D^0 \to K^+K^-)}{\Gamma(D^0 \to K^+\pi^-)} = 9.38 \pm 0.18(\text{stat}) \pm 0.10(\text{sys})\%$ and $\frac{\Gamma(D^0 \to \pi^+\pi^-)}{\Gamma(D^0 \to K^+\pi^-)} = 3.686 \pm 0.076(\text{stat}) \pm 0.036(\text{sys})\%$, comparing favorably with the current best measurement[8]. In the analysis, the D^0 candidate is combined with a charged slow pion to form a D^* meson; in this way, backgrounds are reduced, and the charge of the slow pion from the D^* decay serves as an unbiased tag of the D^0 flavor. Examples of the reconstructed decays are shown in Fig. 7.

The CP violating decay rate asymmetries $A = \frac{\Gamma(D^0 \to f) - \Gamma(\bar{D}^0 \to f)}{\Gamma(D^0 \to f) + \Gamma(D^0 \to f)}$ are also mea-
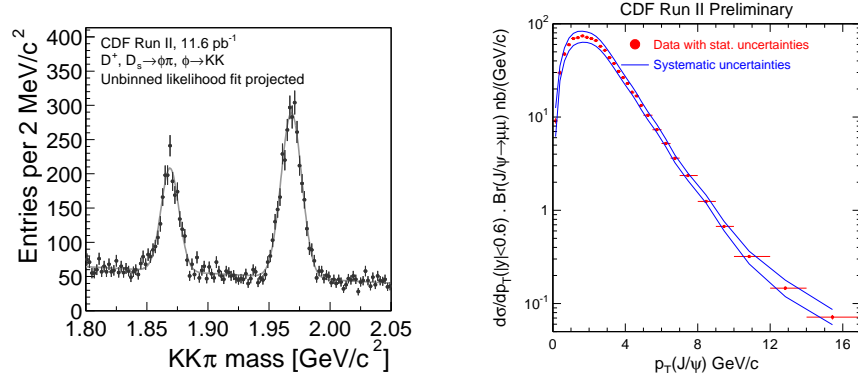
Fig. 6.   *Left:* The reconstructed $D^+ \to \phi\pi^+$ and $D_s^+ \to \phi\pi^+$ mass distribution. *Right:* The inclusive J/ψ cross section differential in p_T for $|y(J/\psi)| < 0.6$.
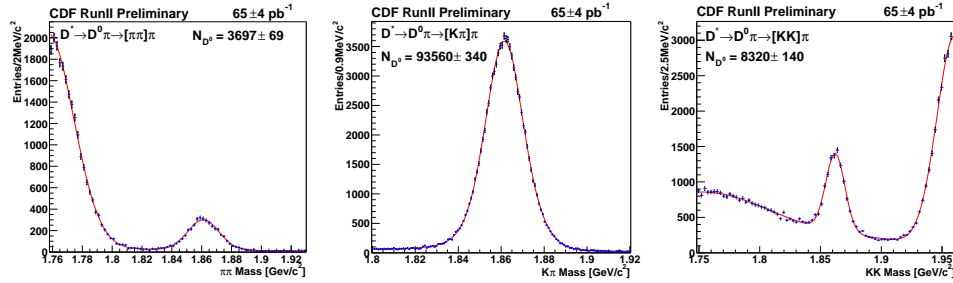

Fig. 7.   Reconstructed D^0 decay modes for branching ratio and CP asymmetry measurements. Note that in the KK (right) and $\pi\pi$ (left) modes the reflections are well separated.

sured. It is found that $A(D^0 \to K^+K^-) = 2.0 \pm 1.7(\text{stat}) \pm 0.6(\text{sys})\%$ and $A(D^0 \to \pi^+\pi^-) = 3.0 \pm 1.9(\text{stat}) \pm 0.6(\text{sys})\%$, comparable to previous measurements[9].

3.1.4. *Search for the FCNC Decay $D^0 \to \mu^+\mu^-$*

The search for the flavor changing neutral current (FCNC) decay $D^0 \to \mu^+\mu^-$ is another example of an analysis that greatly benefits from the SVT trigger, by providing the well measured normalization mode $D^0 \to \pi^+\pi^-$. The branching ratio is $\mathcal{O}(10^{-13})$ in the Standard Model, but can be enhanced up to $\mathcal{B}(D^0 \to \mu^+\mu^-) \simeq 3.5 \cdot 10^{-6}$ in R-parity violating models of Supersymmetry.

In a data sample corresponding to an integrated luminosity of 69 pb^{-1} no candidate event is observed (Fig. 8) with 1.7 ± 0.7 background events expected. After correcting for relative acceptance an upper limit of $\mathcal{B}(D^0 \to \mu^+\mu^-) \leq 2.4 \cdot 10^{-6}$ at 90% CL is set, improving the current best limit[10] of $4.1 \cdot 10^{-6}$.
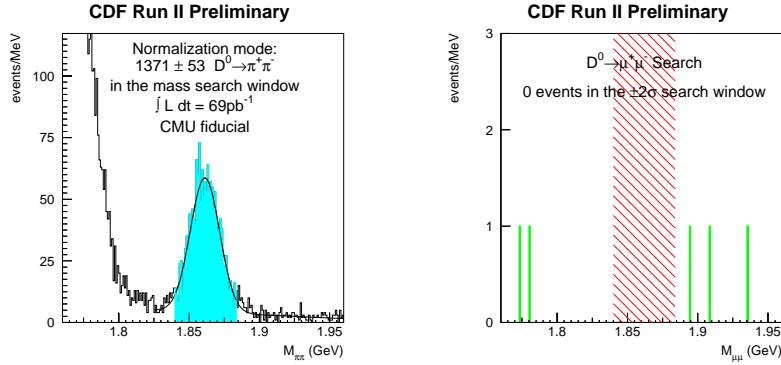
Fig. 8.   Search for $D^0 \to \mu^+\mu^-$. *Left:* Mass spectrum for the normalization mode $D^0 \to \pi^+\pi^-$; the search window is indicated by the shaded area. *Right:* Dimuon candidate events; the search window is indicated by the hatched area.

3.1.5. *Measurement of the J/ψ Cross Section*

One of the surprises of Run I was the direct production cross section for J/ψ and $\psi(2S)$ mesons[11], which turned out to be orders of magnitude larger than the theoretical expectation in the Color Singlet Model. While later calculations within the framework of non-relativistic QCD, including intermediate color octet states, are in broad agreement with the data, there is continued interest in the subject; in particular measurements of the J/ψ and $\psi(2S)$ polarization appear to be in conflict with the theory, albeit not with convincing statistical significance[12].

For Run II the muon trigger momentum thresholds at CDF were lowered to $\geq 1.4\,\mathrm{GeV}$, thus allowing to trigger on J/ψ's at rest for the first time. Using a data sample of $39.7\,\mathrm{pb}^{-1}$ the inclusive differential cross section in bins of the J/ψ transverse momentum has been measured for J/ψ rapidities $|y(J/\psi)| < 0.6$ (Fig. 6). The region $p_T < 5\,\mathrm{GeV}$ is covered for the first time. The total cross section has been determined to be $\sigma(p\bar{p} \to J/\psi X, |y(J/\psi)| < 0.6) \cdot \mathcal{B}(J/\psi \to \mu^+\mu^-) = 240 \pm 1(\mathrm{stat})^{+35}_{-28}(\mathrm{sys})\,\mathrm{nb}$.

Future measurements will include the determination of the prompt production cross section; the inclusive cross section includes J/ψ's from b decays amounting to anything between 0% at small p_T and 50% at large p_T. The prompt J/ψ cross section has contributions from χ_c and $\psi(2S)$ as well as the direct component, which has been measured[13] to be $64 \pm 6\%$ of the prompt cross section in Run I. In addition, more precise data at large p_T, polarization measurements, and similar measurements of $\psi(2S)$, $\Upsilon(1S)$, $\Upsilon(2S)$, and $\Upsilon(3S)$ production will shed further light on the production mechanisms for heavy vector mesons.

3.2. *Beauty*

The major advantage of hadron colliders in the area of b physics is the huge production cross section: $\sigma_{b\bar{b}} \simeq 100\,\mu\mathrm{b}$ at $\sqrt{s} = 2\,\mathrm{TeV}$, compared to $\simeq 1\,\mathrm{nb}$ for e^+e^- colliders running on the $\Upsilon(4S)$ resonance. Making use of this advantage requires
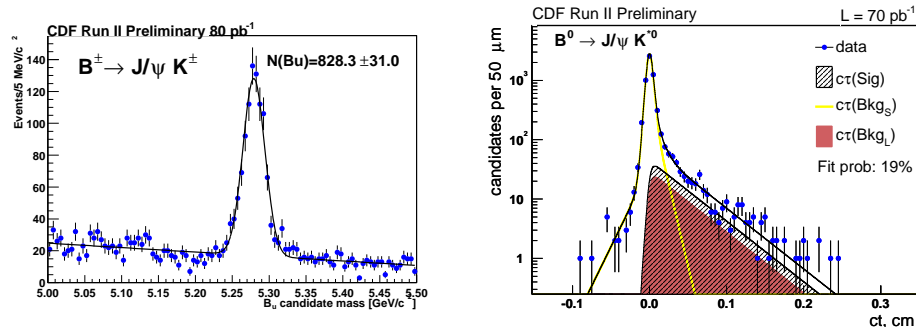
Fig. 9. *Left:* B^+ signal reconstructed in the $J/\psi K^+$ channel. *Right:* The proper decay length distribution of B^0 candidate events. The result of the maximum likelihood fit is overlaid.

a very sophisticated trigger system, which is available in Run II. Another benefit of experiments at hadron colliders is the accessibility of all species of b hadrons — hadron colliders are a unique laboratory for the study of the B_s, B_c, and Λ_b. An extensive review of the Run II prospects can be found in Ref. 14.

Although most of the important measurements related to the Cabibbo-Kobayashi-Maskawa matrix, CP violation, and B_s mixing require significantly larger amounts of data than available to date, a number of competitive benchmark measurements have already been performed.

3.2.1. *Measurement of B Meson Masses and Lifetimes in Exclusive J/ψ Modes*

The masses of the groundstate B mesons have been determined in the exclusive J/ψ decay modes, $B^+ \rightarrow J/\psi K^+$ (Fig. 9), $B^0 \rightarrow J/\psi K^{*0}$, and $B_s^0 \rightarrow J/\psi \phi$, using a data sample corresponding to $80\,\mathrm{pb}^{-1}$. The results for the B^+ and B^0, $m(B^+) = 5279.32 \pm 0.68(\mathrm{stat}) \pm 0.94(\mathrm{sys})\mathrm{MeV}$ and $m(B^0) = 5280.30 \pm 0.92 \pm 0.96\mathrm{MeV}$ compare favorably with present world averages[6]: $m(B^+) = 5279.0 \pm 0.5$ MeV and $m(B^0) = 5279.4 \pm 0.5$ MeV. The B_s^0 measurement, $m(B_s^0) = 5265.50 \pm 1.29 \pm 0.94$ MeV, constitutes the world best measurement (PDG[6]: $m(B_s^0) = 5269.6 \pm 2.4$ MeV).

The same decay modes have been used to measure B meson lifetimes. From an unbinned likelihood fit to the proper decay length the following lifetimes are extracted: $c\tau_{B^+} = 470 \pm 20 \pm 6\mu$m, $c\tau_{B^0} = 425 \pm 28 \pm 6\mu$m, and $c\tau_{B_s} = 379 \pm 59 \pm 6\mu$m. The proper decay length distribution for the B^0 sample is shown in Fig. 9.

3.2.2. *Hadronic Decays*

A large number of additional exclusive b hadron decays have been identified in the early Run II data, thanks to the flexible trigger scheme of the upgraded CDF detector, including for example the purely hadronic decays $B \rightarrow K\pi/\pi\pi/KK$, $B_s \rightarrow D_s^{(*)}\pi$ with $D_s \rightarrow \phi\pi$ and $\phi \rightarrow KK$, $B^\pm \rightarrow \phi K^\pm$, and $\Lambda_b \rightarrow \Lambda_c^+\pi^-$ with $\Lambda_c^+\pi^- \rightarrow pK^-\pi^+$, and will be used for a rich b physics program. The observed signal for $\Lambda_b \rightarrow \Lambda_c^+\pi^-$ is shown in Fig. 10. At the time of writing, this is the largest sample
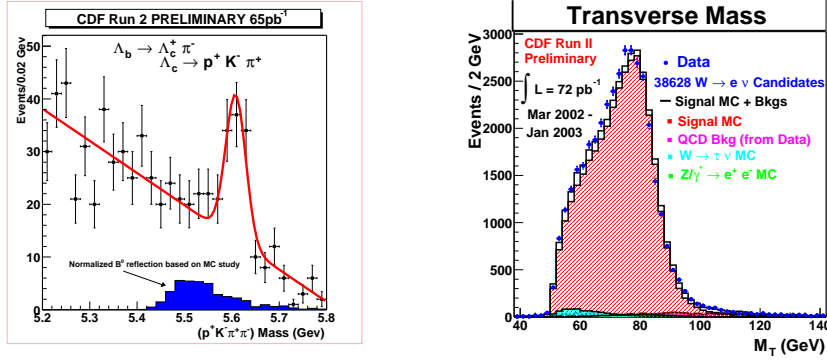
Fig. 10.   *Left:* Observation of $\Lambda_b \to \Lambda_c^+ \pi^-$ signal. *Right:* Transverse mass distribution for $W \to e\nu$ candidate events, overlaid with the expected shape for background and signal.

of fully reconstructed Λ_b's in existance. In the future, beautiful baryons may turn out to be an excellent laboratory for testing the Heavy Quark Effective Theory.

4. Electroweak and Top Physics

A couple of Run II benchmark measurements are expected from the electroweak sector, e.g. the precise determination of the W boson mass. W's and Z's are collected in large numbers and very efficiently in all possible decay channels. Fig. 10 and 12 show examples of W signals in the e and τ channels, and the good understanding of remaining backgrounds. The W cross section has been measured in all three lepton channels[15] (in the electron channel $\sigma_W \cdot \mathcal{B}(W \to e\nu) = 2.64 \pm 0.01(\text{stat}) \pm 0.09(\text{sys}) \pm 0.16(\text{lum})$ nb), and is in good agreement with next-to-next-to-leading order QCD calculations $(2.731 \pm 0.002$ nb$)$. Good agreement is also found between measurements of the Z cross section in the ee and $\mu\mu$ channel and a NNLO prediction. A compilation of the cross section measurements is shown in Fig. 11.

The ratio of the couplings of the W to the τ and e has been measured (Fig.12), which is sensitive to other final states involving τ's and missing transverse energy (charged Higgs decays, production of SUSY particles at large $\tan\beta$). CDF's capabilities to collect large samples of high p_T τ's are greatly enhanced in Run II due to the possibility to trigger on hadronic τ decays.

The reaction $p\bar{p} \to l^+l^-$, where l stands for an isolated high p_T electron or muon, is mediated by virtual photons at low invariant masses $M_{l^+l^-}$, by the Z^0 around the Z pole, and by γ-Z interference. The presence of both vector and axial-vector couplings of electroweak bosons to fermions in the process $q\bar{q} \to Z^0/\gamma^* \to l^+l^-$ gives rise to an asymmetry in the polar angle θ of the electron momentum in the center of mass frame of the lepton pair. The forward-backward asymmetry is defined as $A_{FB} = (N_F - N_B)/(N_F + N_B)$, where N_F (N_B) is the number of forward (backward) events with positive (negative) $\cos\theta$. A_{FB} is a direct probe of the relative strength of the vector and axial-vector couplings. In addition, A_{FB} constrains the properties of
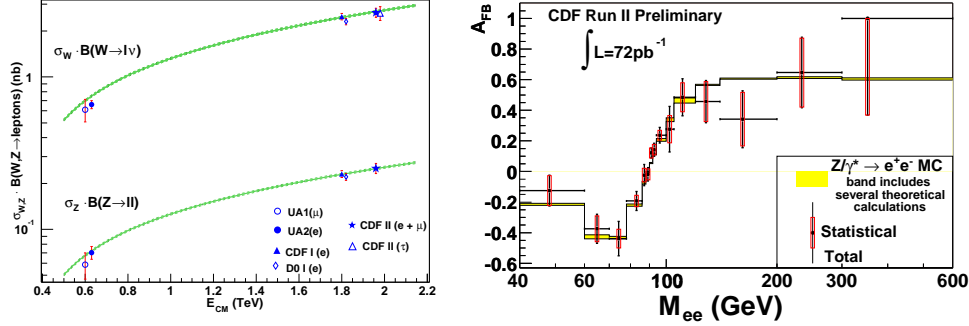
Fig. 11. *Left: Cross section measurements for the W and Z boson together with the NNLO prediction. Right:* Measurement of the forward-backward asymmetry A_{FB} of electron positron pairs. Predictions by the PYTHIA Monte Carlo simulation are shown as a band.
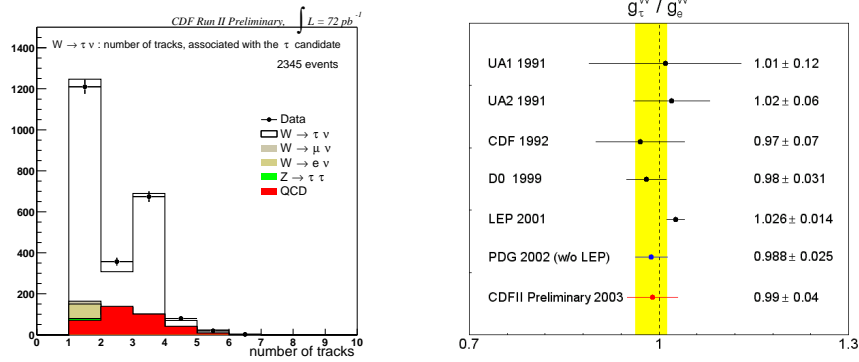

Fig. 12. *Left:* Signal for $W \rightarrow \tau\nu$ seen in the track multitplicity distribution for the τ candidates. *Right:* The ratio of the couplings of the W to the τ and e as measured by CDF compared to earlier measurements.

any additional heavy neutral gauge boson, and is complementary to a direct search via deviations in the cross section measurement. Using 5438 e^+e^- pairs collected in a data sample corresponding to 72 pb^{-1}, the forward-backward asymmetry is measured for $40 < M_{e^+e^-} < 600$ GeV. The result is shown in Fig. 11, and agrees well with theoretical predictions.

Top Production The Tevatron experiments are to date the only places where direct measurements of the top quark can be performed. At the Tevatron top quarks are produced predominantly in pairs through the QCD processes $q\bar{q} \rightarrow t\bar{t}$ (85%) and $gg \rightarrow t\bar{t}$ (15%). Single top quark production via the electroweak vertex Wtb is predicted with about half the cross section, but — with final states difficult to extract from the background — is only expected to be observable later in Run II. With 2 fb^{-1} of integrated luminosity, cross section measurements with a precision of 7% and 20% are expected for $t\bar{t}$ and single top production, respectively.

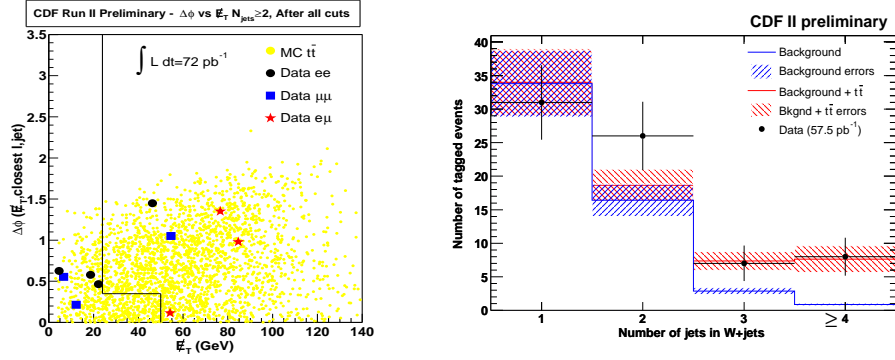Within the Standard Model the top quark decays almost exclusively into Wb.

Fig. 13.   *Left:* The five $t\bar{t}$ dilepton candidates in the plane $\Delta\phi(\not{E}_T$, nearest l or $j)$ vs. $\not{E}_T$ in comparison with the Herwig $t\bar{t}$ Monte Carlo simulation. *Right:* Number of events in the $W+$ jets sample with at least one b tag; the 3 and ≥ 4 bins are used to extract $\sigma_{t\bar{t}}$.

In the dilepton channel, both W's decay leptonically to e or μ; the branching ratio is small (5%), but so are backgrounds. In the "lepton + jets" channel one W decays leptonically and the other one hadronically; the branching ratio is $\simeq 30\%$. Fig. 13 shows the candidate events in both channels, for an integrated luminosity of 72 pb^{-1} and 58 pb^{-1}, respectively. The cross section is measured to be $\sigma_{t\bar{t}} = 5.3 \pm 1.9(\text{stat}) \pm 0.8(\text{sys}) \pm 0.3(\text{lum})$ pb (lepton + jets) and $\sigma_{t\bar{t}} = 13.2 \pm 5.9(\text{stat}) \pm 1.5(\text{sys}) \pm 0.8(\text{lum})$ pb (dilepton). These results are consistent with the next-to-leading order QCD prediction[16] of $\sigma_{t\bar{t}} = 6.70^{+0.71}_{-0.88}$ pb, which is about 30% higher than the corresponding Run I value due to the higher center of mass energy.

5. QCD

Hadronic jets are one of the key signatures in hadronic collider physics, and probe the highest momentum transfer region currently accessible at any collider. A first measurement of the inclusive jet E_T cross section in Run II based on an integrated luminosity of 85 pb^{-1} of data has been performed. The data span the E_T range from 44 to 550 GeV, extending the upper limit by almost 150 GeV compared to Run I. In Fig. 14 the measurement is compared to the NLO QCD expectation determined using the CTEQ 6.1 parameterization[17] of the parton density functions. The systematic uncertainty is dominated by the 5% energy scale uncertainty, which is expected to be reduced to of the order of 1% over the course of Run II.

A measurement of the dijet mass spectrum using 75 pb^{-1} of data is shown in Fig. 15, extending from 180 GeV and falling steeply, with the event with the highest dijet mass at 1364 GeV. The ratio of the cross sections measured in Run I and Run II compares well with QCD calculations, and the Run II cross section is above the Run I measurement by a factor of 1.1 (low mass) to more than 2 (high mass). Performing a simple parameterization of the spectrum, and taking into account the fractional difference between the data and the fit as well as the
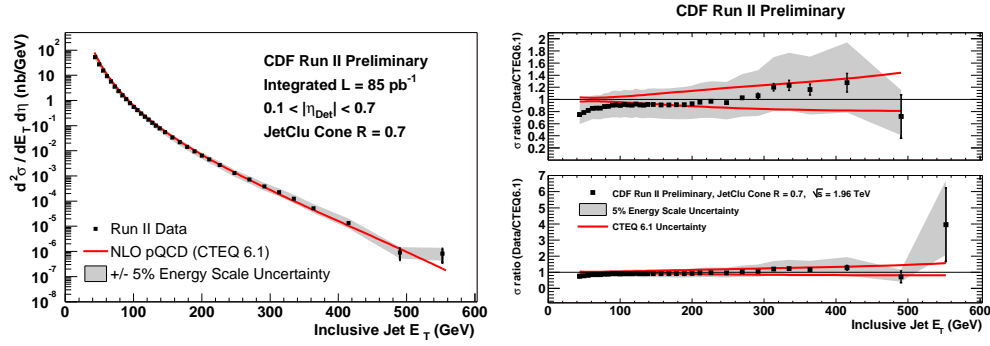
Fig. 14.   *Left:* Measurement of the inclusive jet cross section, compared to the NLO QCD expectation using the CTEQ 6.1 parton density functions. The variation in the cross section due to the 5% energy scale uncertainty is shown as a band. The two lines indicate the uncertainty in the cross section prediction due to the PDF. *Right:* The ratio of data and theory.
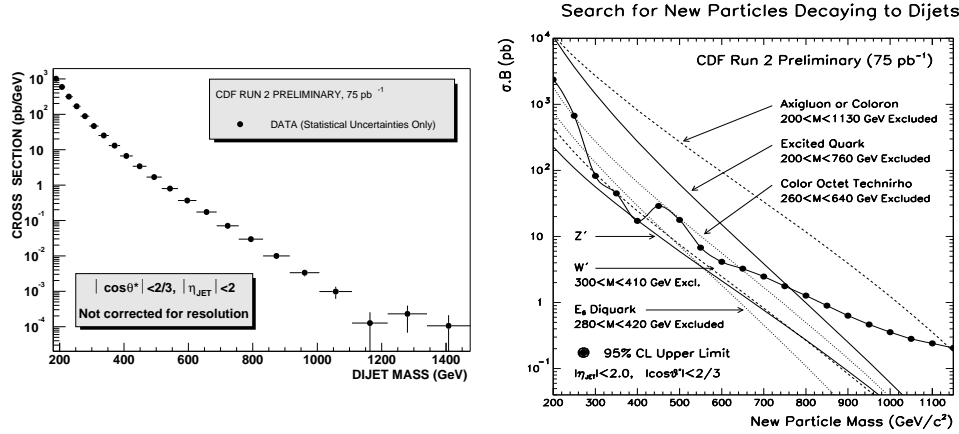

Fig. 15.   *Left:* Dijet mass spectrum. *Right:* 95% CL upper limits on the cross section times branching ratio for narrow dijet resonances, and predictions for axigluons, flavor universal colorons, excited quarks, Color Octet Technirhos, E6 diquarks, W' and Z'.

statistical residuals between the data and the fit, shows that there is no evidence for a new particle compatible with the dijet mass resolution. These data can be used to exclude the production of a variety of particles decaying into dijets. The 95% confidence upper limit for cross section times branching ratio together with predictions for the production of axigluons, flavor universal colorons, excited quarks, Color Octet Technirhos, E6 diquarks, W', and Z' are shown in Fig. 15. All of the exclusion regions are either similar or better than the corresponding Run I limits.

6. Searches

One of the main goals of the Tevatron is to uncover physics beyond the Standard Model. A large number of searches is actively pursued, both in the more traditional model-based approach, where the analysis is optimized for best sensitivity
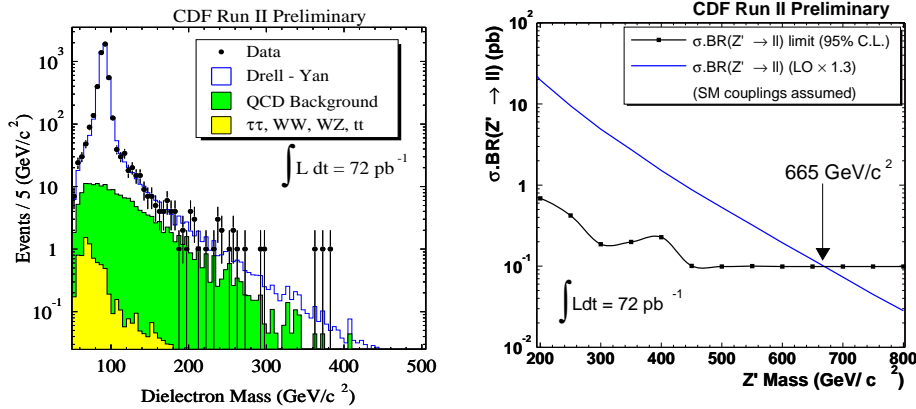
Fig. 16.   *Left:* Drell Yan spectrum in the dielectron channel. *Right:* Limit on Z' production, combining the dielectron and dimuon channels.

with regard to specific predictions, as well as signature-based searches, where the observation of a given event type is compared to Standard Model expectations. A few examples are shown in this section.

The dilepton mass spectrum was analysed to search for anomalies in the high mass region. Additional neutral gauge bosons would show up as resonances in the measured dielectron and dimuon mass spectra (see Fig. 16 for the dielectron spectrum). The data are well described by Standard Model processes, and a limit for the production of a Z' boson is set (Fig. 16) which is comparable to the Run I analyses. A Randall-Sundrum graviton[18] would show up as a spin 2 resonance in the Drell-Yan spectrum. Limits ranging from 205 GeV to 535 GeV are set[19].

An analysis that exploits the new capabilities of the upgraded CDF detector is the search for long lived charged massive particles (CHAMPS). These particles will have a long time of flight through the detector, and the new TOF system provides a sensitivity to higher $\beta\gamma$ than the conventional approach of using energy loss (dE/dx) measurements provided by the drift chamber. If the CHAMP lifetime is long enough to traverse the whole detector, candidate events can be collected using the high p_T muon trigger. The discriminant variable in the analysis is Δ_{TOF}, which is the difference between the measured time of flight for a particle and the time of flight expected for a particle travelling at the speed of light. The observed Δ_{TOF} spectrum in $53\,\mathrm{pb}^{-1}$ of data is shown in Fig. 17, together with the prediction based on a control sample. For a specific SUSY model cross section limits have been set as a function of the stop mass (Fig. 17), yielding a mass limit $M_{stop} > 108\,\mathrm{GeV}$ at 95% confidence level.

7. Conclusions

After a five year shutdown and one year of commissioning, all major components of the CDF detector are operating at or near their design specifications for the Tevatron Run II. All relevant benchmark signals are observed and used both to
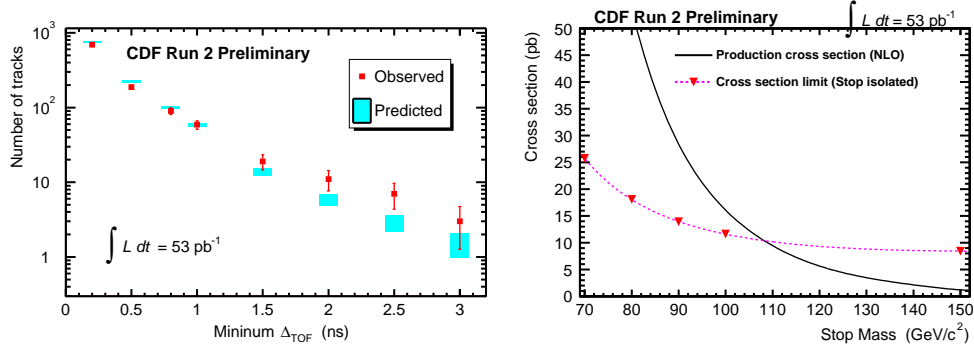
Fig. 17. Search for CHAMPS. *Left:* Observed and predicted number of events as function of Δ_{TOF}. *Right:* Cross section limit as function of stop mass.

characterize the detector performance, and to make several physics measurements. In particular, the data collected lately provide insight into CDF's heavy flavor capabilities. In spite of the still limited accumulated luminosity some measurements already improve the best currently available.

Acknowledgments

I wish to thank my colleagues in CDF who provided most of the material.

1. CDF II Collaboration, *The CDF-II Detector: Technical Design Report*, Fermilab-Pub-96-390-E (1996)
2. A. Meyer, *The CDF Data Acquisition System for Tevatron Run II*, International Conference on Computing in High Energy and Nuclear Physics (CHEP 2001), proceedings and Fermilab-Conf-01-242-E (2001)
3. W. Ashmanskas *et al.*, *Nucl. Instrum. Meth.* **A447**, 218 (2000)
4. B.A. Kniehl and G. Kramer, private communication; B.A. Kniehl, G. Kramer and B. Potter, *Nucl. Phys.* **B597**, 337 (2001)
5. M. Cacciari and P. Nason, private communication; M. Cacciari, M. Greco and P. Nason, *JHEP* **9805**, 007 (1998); M. Cacciari and P. Nason, *Phys. Rev. Lett.* **89**, 122003 (2002)
6. K. Hagiwara *et al.*, *Phys. Rev.* **D66**, 010001 (2002)
7. D. Acosta *at al.*, CDF II Collaboration, *Measurement of the Mass Difference $m(D_s^+) - m(D^+)$ at CDF II*, Fermilab-Pub03/048-E (2003), submitted to *Phys. Rev. D*
8. FOCUS Collaboration, *Phys. Lett.* **B555**, 167 (2003)
9. CLEO Collaboration, *Phys. Rev.* **D65**, 092001 (2002)
10. BEATRICE Collaboration, *Phys. Lett.* **B408**, 469 (1997)
11. CDF Collaboration, *Phys. Rev. Lett.* **79**, 572 (1997)
12. CDF Collaboration, *Phys. Rev. Lett.* **85**, 2886 (2000)
13. CDF Collaboration, *Phys. Rev. Lett.* **79**, 578 (1997)
14. K. Anikeev *et al.*, *B Physics at the Tevatron: Run II and Beyond*, Fermilab-Pub-01-197 (2001)
15. T. Dorigo, *W and Z Cross Sections at the Tevatron*, XXXVIII. Rencontres de Moriond on QCD and High-Energy Hadronic Interactions, proceedings (2003)
16. M. Cacciari *et al.*, CERN-TH-2003-054
17. J. Pumplin *et al.*, *JHEP* **0207**, 012 (2002)
18. L. Randall and R. Sundrum, *Phys. Rev. Lett.* **83**, 3370 (1999)

19. S. Rolli, *Search for New Particles at CDF II*, XXXVIII. Rencontres de Moriond on Electroweak Interactions and Unified Theories, proceedings (2003)